Conclusions from recent pionic–atom experiments [1]

D. Gotta[*], F. Amaro[†], D. F. Anagnostopoulos[**], S. Biri[‡], D. S. Covita[†], H. Gorke[§], A. Gruber[¶], M. Hennebach[*], A. Hirtl[¶], T. Ishiwatari[¶], P. Indelicato[‖], Th. Jensen[‖], E.–O. Le Bigot[‖], J. Marton[¶], M. Nekipelov[*], J. M. F. dos Santos[†], S. Schlesser[‖], Ph. Schmid[¶], L. M. Simons[††,†], Th. Strauch[*], M. Trassinelli[‖], J. F. C. A. Veloso[†] and J. Zmeskal[¶]

[*]*Institut für Kernphysik, Forschungszentrum Jülich, D–52425 Jülich*
[†]*Dept. of Physics, Coimbra University, P–3000 Coimbra, Portugal*
[**]*Dept. of Material Science and Engineering, University of Ioannina, Ioannina, GR–45110, Greece*
[‡]*Institut of Nuclear Research, Hungarian Academy of Sciences, H–4001 Debrecen, Hungary*
[§]*Zentrallabor für Elektronik, Forschungszentrum Jülich, D–52425 Jülich*
[¶]*Stefan Meyer Institut, Austrian Academy of Sciences, A–1090 Vienna*
[‖]*Lab. Kastler Brossel, UPMC–Paris 6, ENS, CNRS; 4 place Jussieu, F–75005 Paris, France*
[††]*Paul Scherrer Institut, Villigen PSI, CH–5232 Villigen, Switzerland*

Abstract. The most recent pionic–hydrogen experiment marks the completion of a whole series of measurements, the main goal of which was to provide conclusive data on pion–nucleon interaction at threshold for comparison with calculations from Chiral perturbation theory. The precision achieved for hadronic shift and broadening of 0.2% and 2%, respectively, became possible by comprehensive studies of cascade effects in hydrogen and other light exotic atoms including results from the last years of LEAR operation. In order to obtain optimum conditions for the Bragg crystal spectrometer, the cyclotron trap II has been used to provide a suitable X–ray source. To characterize the bent crystal spectrometer, the cyclotron trap has been modified to operate as an electron–cyclotron resonance source, from which narrow X–ray transitions are emitted with high intensity from the highly charged ions.

Keywords: Exotic atoms, pion–nucleon intercation, X–ray spectroscopy, crystal spectrometer
PACS: 36.10.-k, 36.10.Gv, 13.75.Gx, 32.30.Rj, 07.85.Nc

INTRODUCTION

Calculations within the modern low–energy approach of QCD – Chiral Perturbation Theory (χPT) – have reached an accuracy of a few per cent. This in turn requires data at a similar level of precision. χPT is based on the fact that the (almost) massless quarks allow a quantitative description by effective degrees of freedom circumventing a treatment based on the elementary constituents quarks and gluons [1]. A fundamental treatment in terms of color QCD is expected to be feasible in future by lattice gauge calculations, but nowadays effective field theories like χPT must be used in the non perturbative regime. Nonetheless, the underlying chiral symmetry arising from the vanishing mass of the

[1] CP1037, 162-177 (2008), *Cold Antimatter Plasmas and Application to Fundamental Physics*, edited by Y. Kania and Y. Yamazaki, ©2008 American Institute of Physics 978-0-7354-0561-5/08

(current) quarks u, d, and s determines the interaction of the effective fields like pions and kaons. They are identified to be the Goldstone bosons originating from the so called spontaneous breaking of chiral symmetry. Basic low–energy theorems are formulated in the chiral limit, i. e., vanishing quark masses. Finite masses as well as electromagnetic interaction are included as perturbation quantifying the breaking of the symmetry. In this scheme, mass and interaction of the "Goldstone bosons" are related to the degree of symmetry breaking [2, 3, 4, 5, 6].

At threshold the interaction of the pion–nucleon system is given by two real numbers, the scattering lengths according to the two isospin combinations $I = 1/2$ and 3/2 occuring for the πN system. The isospin even and odd combinations read

$$a^+ = \frac{1}{3}\,(a_{1/2} + 2a_{3/2}) \tag{1}$$

$$a^- = \frac{1}{3}\,(a_{1/2} - a_{3/2}). \tag{2}$$

The leading order result of χPT for a^+ and a^- is obtained from current algebra, which revealed already as an important consequence of the underlying chiral symmetry a simple relation between the isospin contributions [7, 8, 9]. E. g., it causes the isoscalar combination a^+ to vanish exactly:

$$a^+ = 0 \tag{3}$$

$$a^- = a_{1/2} = -2a_{3/2} = -0.079/m_\pi \tag{4}$$

Deviations from these values represent the higher orders in χPT [10, 11, 12, 13, 14, 15, 16, 17, 18].

The scattering lengths $a^\pm$ are related to elementary πN reactions accessible by experiment:

$$a^\pm = \frac{1}{2}\,(a_{\pi^- p\to\pi^- p} \pm a_{\pi^+ p\to\pi^+ p}). \tag{5}$$

In the limit of isospin symmetry, the intercations with charged pions yield directly the charge exchange process

$$a_{\pi^- p\to\pi^- p} - a_{\pi^+ p\to\pi^+ p} = -\sqrt{2}\,a_{\pi^- p\to\pi^0 n}. \tag{6}$$

The scattering lengths $a_{\pi^- p\to\pi^- p}$ and $a_{\pi^- p\to\pi^0 n}$ are related to the ground state strong–interaction shift ε and broadening Γ of the pionic–hydrogen atom and are measured by means of energy and line width of characteristic X–radiation from the πH atom (Fig. 1). Shift and width may be expressed by Deser–type formulae[2] [19, 20, 21]:

$$\frac{\varepsilon_{1s}}{B_{1s}} = -\frac{4}{r_B}\,a_{\pi^- p\to\pi^- p}(1+\delta_\varepsilon) \tag{7}$$

---

[2] $q_0 = 0.1421\,fm^{-1}$ is the centre–of–mass momentum of the π^0 in the charge–exchange reaction $\pi^- p \to \pi^0 n$ and $P = 1.546 \pm 0.009$ [22] the branching ratio of charge exchange and radiative capture (Panofsky ratio).

$$\frac{\Gamma_{1s}}{B_{1s}} = 8\frac{q_0}{r_B}(1+\frac{1}{P})[a_{\pi^- p\to\pi^0 n}(1+\delta_\Gamma)]^2. \quad (8)$$

Obviously $\varepsilon_{1s} \propto a^+ + a^-$ and, in the limit of isospin invariance, $\Gamma_{1s} \propto (a^-)^2$ holds in leading order. The contribution of charge exchange to the total width is obtained after correction for radiative capture ($\pi^- p \to \gamma n$) using the well known Panofsky ratio P [22]. Electromagnetic and higher order corrections encoded by the parameters δ_ε and δ_Γ have been continuously improved especially within the framework of χPT [13, 15, 23, 24, 25, 26, 27].

More important quantities are closely related to the πN scattering lengths. Using the Goldberger–Miyazawa–Oehme (GMO) sum rule, the isovector scattering length a^- yields the πN coupling constant $f^2_{\pi N}$ [28, 29, 30]. The coupling constant $f^2_{\pi N}$ itself may be used to determine the induced pseudovector coupling g_p, a quantity accessible otherwise by muon capture experiments $\mu^- p \to n\nu_\mu$ [31, 32, 33]. The electric dipole amplitude E_{0+} for π^- photo production $\gamma n \to \pi^- p$ is also directly connected to a^- [9, 34]. The isoscalar contribution a^+ is related to the πN σ–term which is an important contribution to the nucleon mass [35, 36].

χPT, being an effective field theory, contains at any order of expansion coupling constants, so called low–energy constants (LECs), which represent the short range part of the interaction. The LECs have to be determined from experiment and not all of them are known to sufficient accuracy. In the case of the πH ground state shift, the precision for $a^+ + a^-$ is limited to $\pm 3\%$ by one particular LEC f_1 [25], whereas experiment is one order of magnitude more precise (see below and [37, 38]). The LEC f_1 does not appear in the expression relating Γ_{1s} to a^- and, hence, the theoretical uncertainty is quoted to be only $\pm 0.2\%$ [26].

Combining πH ground state shift, broadening and πD ground state shift, the scattering lengths a^+ and a^- are overdetermined, because in leading order $\varepsilon_{1s}(\pi\mathrm{D}) \propto a^+$ [39, 40, 41, 42, 43, 44]. Precise πH and πD data together even yield a constraint on f_1 [45].

Because of the almost cancellation of the $\pi^- p$ and $\pi^- n$ interaction, the πD system shows an outstanding sensitivity to isospin breaking contributions for reactions involving charged pions [45, 46]. The hadronic broadening in πD is related by detailed balance to s–wave pion production in the reaction $pp \to d\pi^+$ [47]. Consequently, to improve on the results of previous measurements [48, 49], a high–precision measurement of the πD system was part of the experimental program [50, 51].

ATOMIC CASCADE

Pionic hydrogen

After capture into high–lying atomic states, the de–excitation cascade of pionic hydrogen is governed by collisional processes. Due to a finite target density numerous elastic and inelastic collisions occur leading among others to Stark mixing and Coulomb de–excitation. The upper part of the atomic cascade is determined by external Auger effect and Coulomb de–excitation. Between low–lying states, X–ray transitions dominate (Fig. 1).

Due to the fact that exotic hydrogen is electrically neutral, Stark mixing plays an outstanding role, because the atom approaches easily the nuclei of the target molecules experiencing there a strong Coulomb field. In the presence of strong interaction, the mixing of different angular momentum states ℓ for given main quantum number n leads to nuclear reactions whenever an s–wave contribution is admixed and, consequently, the X–ray cascade is strongly depleted with increasing density [52]. Typical line yields for pionic hydrogen are a few per cent only at target densities equivalent to pressures of a few bar [53]. More details on capture, cascade and strong–interaction effects may be found in [54, 55].

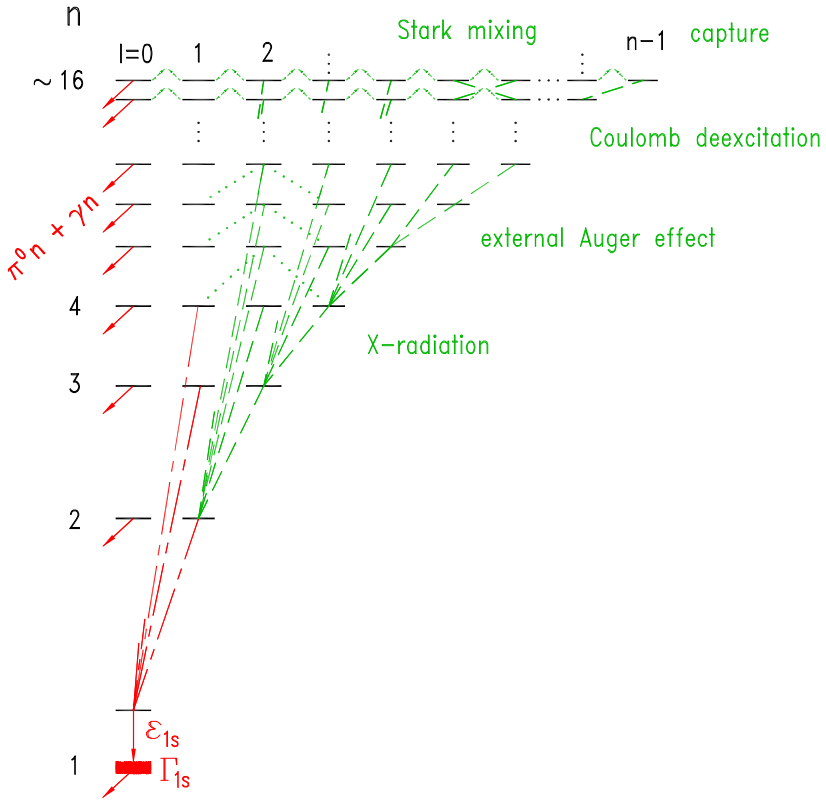

FIGURE 1. Atomic cascade in pionic hydrogen. In this experiment, the transitions πH$(2p-1s)$, πH$(3p-1s)$, and πH$(4p-1s)$ with the energies of 2.437, 2.885, and 3.043 keV have been studied. The hadronic shift ε_{1s} is given by the difference $E_{exp} - E_{QED}$ of the measured and calculated purely electromagnetic energy for the X–ray transition. Hadronic shift and broadening Γ_{1s} of the ground state are about + 7 and 1 eV [37], respectively. In the case of πH, the positive shift reveals the attractive $\pi^- p$ interaction. For πD, the sum of the $\pi^- p$ and $\pi^- n$ interaction leads to a small negative value for the shift (≈ -2.5 eV), where the broadening is 1.2 eV, i. e., comparable to the πH case [48, 49].

Coulomb de–excitation is particularly important in the case of the line width measurement. In distributing the energy gain of a cascade step as kinetic energy to the collision partners (generally the πp system and an H atom from an H_2 molecule), the pionic hydrogen atom is accelerated. The acceleration was observed directly for the first time from a broadening in neutron time–of–flight spectra stemming from the two–body reaction

$\pi^- p \rightarrow \pi^0 n$ [59, 60]. Alike a Doppler broadening of the X–ray line must be expected from such a moving source and has to be quantified preciseley for a proper extraction of the hadronic width. Whereas charge exchange occurs from *ns* states, mainly with $n = 3-5$ of the $\pi^- p$ system, in the case of X–ray emission *np* levels are the initial states and preceding cascade steps may be completely different. Therefore, a dedicated study for the X–ray case is necessary.

Acceleration caused by Coulomb de–excitation is not included in the standard cascade model (SCM), where the kinetic energy is a state independent parameter fitted to the measured X-ray line yields [56]. In the extended cascade model (ESCM), the development of the kinetic energy through the de–excitation steps has been included [57, 58]. The kinetic energy distribution for the πH atom being in an atomic state (n,ℓ) is obtained by following the competition of acceleration by Coulomb de–excitation and deceleration in the foregoing cascade steps. In order to test the predictions of the ESCM, Coulomb de–excitation was studied by measuring the $3p-1s$ transition in muonic hydrogen, where Doppler broadening is better visible because of the absence of strong interaction (see below).

Another process to be considered is molecular formation, possibly affecting the extraction of the hadronic shift. As known from muon–catalyzed fusion, complexes like $(\mu\mathrm{H})_{nl}+\mathrm{H}_2 \rightarrow [(pp\mu)_{nvj}\ p]2e^-$ are formed during the collision [61]. Similarly, molecular formation should occur with pions. The quantum numbers *v* and *j* denote vibrational and total angular momentum of the 3–body molecular state. Though the 3–body system $(pp\pi)_{nvj}$ is assumed to de–excite mainly by Auger emission it cannot be excluded beforehand that a fraction of the πH atoms bound into such molecules decays radiatively to the ground state. Small line shifts – here to lower energies – cannot be resolved and, hence, falsify the extracted hadronic shift [62, 63, 64]. It is assumed that the formation rate depends on the number of collisions, i. e., on density, and consequently a density dependent shift of the line center indicates radiative de–excitation of molecules. Therefore, in the experiment a possible energy dependence of the X–ray energy was thoroughly studied.

Light pionic atoms

Exotic–atom X–ray transitions are usable as calibration standards [65]. In low and medium *Z* atoms the electron shell is completely removed by Auger emission when refilling of electrons from neighbouring atoms is suppressed [66, 67]. Hence, in the medium part of the cascade the pionic atom is a hydrogen–like system, and because the small overlap of the pion and nucleus wave functions, strong–interaction effects are negligibly small. Level energies are then calculable from QED to a precision of a few meV [68]. This was exploited for the transition combination $\pi\mathrm{H}(3p-1s)$ and $\pi^{16}\mathrm{O}(6h-5g)$.

Radiative widths in exotic atoms are much smaller than in electronic systems which suggests to use the πO transition also for the determination of the apparative response. However, for molecules at first the binding electrons are quickly removed, while the heavy and highly charged ions are still at a distance of about the molecular bond length.

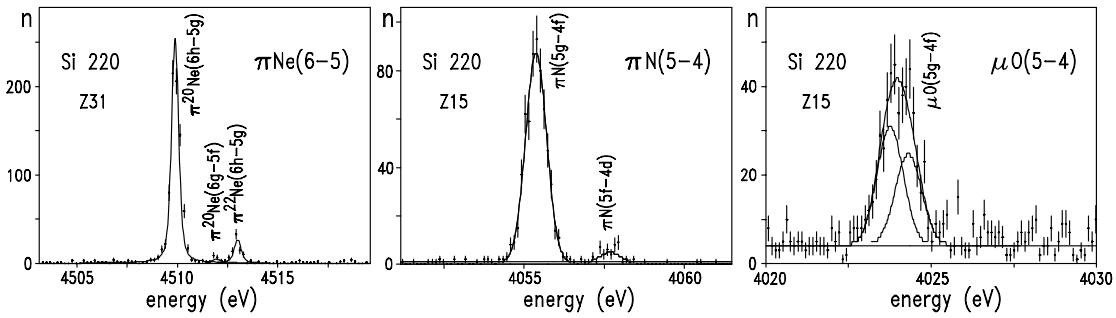

FIGURE 2. Comparison of the line widths of πNe, πN, and μO transitions. The additional broadening for the atoms formed with molecules is due to a Doppler broadening caused by Coulomb explosion (from [69]).

Finally, the pion is attached to one of the ions which, due to Coulomb repulsion, is accelerated. The subsequent X–ray transition is then Doppler broadenend. Coulomb explosion was observed directly by comparing the line widths of X–ray transitions in pionic neon to pionic nitrogen and muonic oxygen [69] (Fig. 2).

Consequently, a precision determination of the crystal resolution would be restricted to noble gases, however, at first transition energies do not fit and, secondly, count rates are very limited. Therefore, a new approach using highly charged ions had to be used (see below), because intense γ rays from radioactive sources are also not available in the few keV range (see below and [65]).

EXPERIMENT

X–ray energies of the ground–state transitions in muonic and pionic hydrogen and deuterium are 2–3 keV, where hadronic shift and width are of the order of eV. Therefore, a reflection–type spectrometer must be used equipped with quartz or silicon Bragg crystals, which are the only manageable materials reaching a resolution of about 10^{-4} in this energy range.

The determination of the hadronic effects at the per cent level requires both high statistics and ultimate energy resolution, which is usually mutually exclusive. Even with a high flux facility as available at the Paul Scherrer Institut (PSI), exotic–atom X–ray rates are at the lower edge for ultimate–resolution spectroscopy. Hence, a compromise has to be found for setting up a high–resolution device and an acceptable count rate. The best approach is a Johann–type spectrometer using spherically bent crystals (Fig. 3. Because the overall efficiency of such a spectrometer is still very low, the cyclotron trap is essential to provide a bright X–ray source. A combination of cyclotron trap and Johann spectrometer was used first at LEAR in the measurement of the Lα transitions (1.7 and 2.4 keV) in antiprotonic hydrogen and deuterium [70].

FIGURE 3. Setup in the πE5 area at PSI of cyclotron trap, crystal spectrometer and X–ray detector (CCD) for the πH$(3p-1s)$ measurement. The massive concrete shielding is essential to achieve a good peak–to–background ratio.

X-ray source

PSI provides low–energy pions of high intensity which are produced by means of the 590 MeV proton beam (up to 1.8 mA). The short πE5 beam line, set up for 112 MeV/c momentum, leads up to a few $10^8\,\pi^-/s$ to the experimental area, where the pions enter the gap between two superconducting coils (cyclotron trap II). The cyclotron trap provides a magnetic field with focussing properties which, with the help of degraders, guides the beam towards its center [71] (Fig. 4).

To study the cascade effects, a wide range must be covered for the hydrogen density. This was achieved by using a cryogenic target. At a gas pressure of 1 bar, about 0.5% of the incoming pions are stopped in a thin–walled hydrogen filled cell. The stop efficiency increases linearly with density up to 30 bar pressure equivalent, counterbalancing the decreasing X–ray line yields. The cell diameter of about 5 cm represents the extension of the X–ray source. The large gap of the cyclotron trap II allows also an efficient formation of muonic atoms. The muons originate from the decay of slow pions inside the magnet's chamber. The stop efficiency for muons is about a factor of 20 lower than for pions, which is partly compensated by the higher μH line yields [72].

Due to pion absorption a high neutron induced background occurs. With a massive

concrete ıieved in
the X–ra

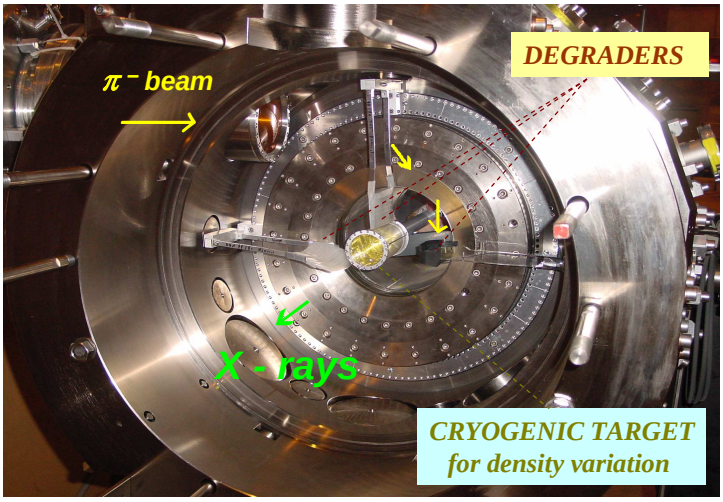

FIGURE 4. Interior of the cyclotron trap with the second coil and its iron yoke removed. Degraders reduce the momentum that after about 2 turns a fraction of the beam stops in gas of the target cell. The wall of the cell is made of 50 μm thick KAPTON foil. The exit window towards the crystal spectrometer has a thickness of 7.5 μm.

Crystal spectrometer

A bent crystal setup (Johann–type spectrometer) allows the simultaneous measurement of an energy interval, the width of which is given by the extension of the X–ray source in the direction of dispersion. A crystal diameter of about 6–10 cm and a curvature of about 3 m constitutes a compromise between count rate and abberations due to the finite size of the crystal. The use of spherically bent crystals leads in addition to a partial vertical focussing enhancing further the count rate. The total height of the reflection of about 100 mm is then mostly covered by the detector's vertical extension of 75 mm. The efficiency of the spectrometer, given by geometry and reflectivity of the crystal, is of the order 10^{-6}. Count rates of 10–50 per hour were achieved for the various pionic–hydrogen transitions.

In the direction of dispersion, the detector width has to cover about the width of the target window. E. g., for the πH$(3p-1s)$ transition at 2.885 keV and using a Si 111 crystal yielding a Bragg angle of 43.2°, the width of the detector array of 50 mm corresponds to 45 eV. This allows the simultaneous measurement of the π^{16}O$(6h-5f)$ transition of 2.880 keV used for energy calibration (Fig. 8). At higher target densities, when oxygen freezes out, hydrogen and oxygen were measured alternately. Because of the detector size, none of the spectrometer parts had to be moved thus preserving the energy calibration.

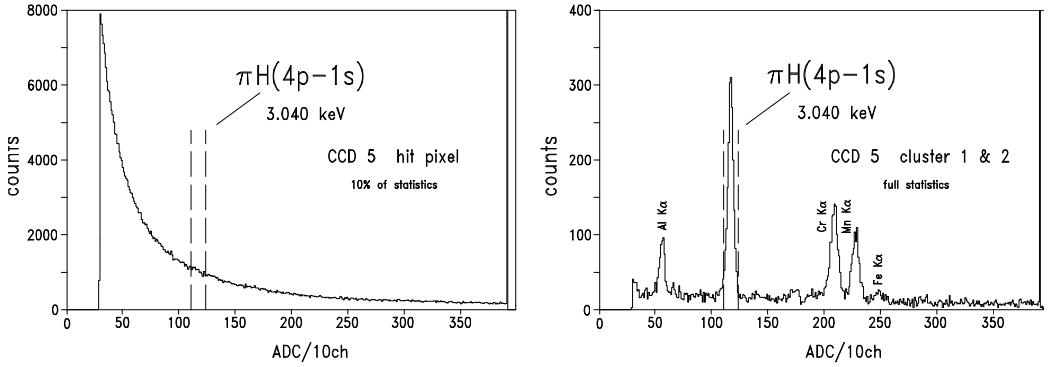

FIGURE 5. ADC (charge) spectra from the πH$(4p-1s)$ experiment: raw data (left) and data after eliminating clusters except single and adjacent two–pixel hits (right). Position spectra are then generated only from the events of the cleaned data lying inside the ADC cut corresponding to the energy of the πH$(4p-1s)$ X–rays.

X–ray detector

At facilities producing hadron induced background, charge–coupled devices (CCDs) are most suitable X–ray detectors because they combine a build–in two–dimensional position sensitivity with the good energy resolution owing to semiconductor devices of 200 eV or better at a few keV. Where X–rays produce short–ranged photo electrons depositing charge in one or two pixels only, background events stemming from high energy photons following neutron capture cause larger patterns. As the pixel structure allows a reconstruction of the hit pattern, background is reduced by at least an order of magnitude (Fig. 5). In the recent pionic–atom experiment, a 2×3 array was used built up of 6 CCDs with 600×600 pixels of 40 μm size and cooled to -100°C [73]. The CCD's cryostat volume was separated from the spectrometer vacuum by a 5 μm thick MYLAR window.

ECRIT

The response function of a bent crystal spectrometer is given by the convolution of the geometrical imaging and the intrinsic properties of the crystal material. The total reflection is the sum over all source points contributing to the reflection. The intrinsic properties are given by the so called rocking curve, which is reliably calculable for plane crystals by diffraction theory [74]. The geometry of the spherically bent crystal setup is modeled by Monte Carlo ray–tracing calculations. Rocking curve, assuming an ideal material, and ray tracing yields the "ideal" response of the setup. Due to the non trivial superposition of geometry and crystal properties an experimental verification of the response is mandatory.

In order to quantify precisely deviations from the ideal case, systematic high–statistics studies of the crystal response funcion were performed. For the first time narrow X–ray lines from highly ionised atoms, produced in a dedicated device, have been used.

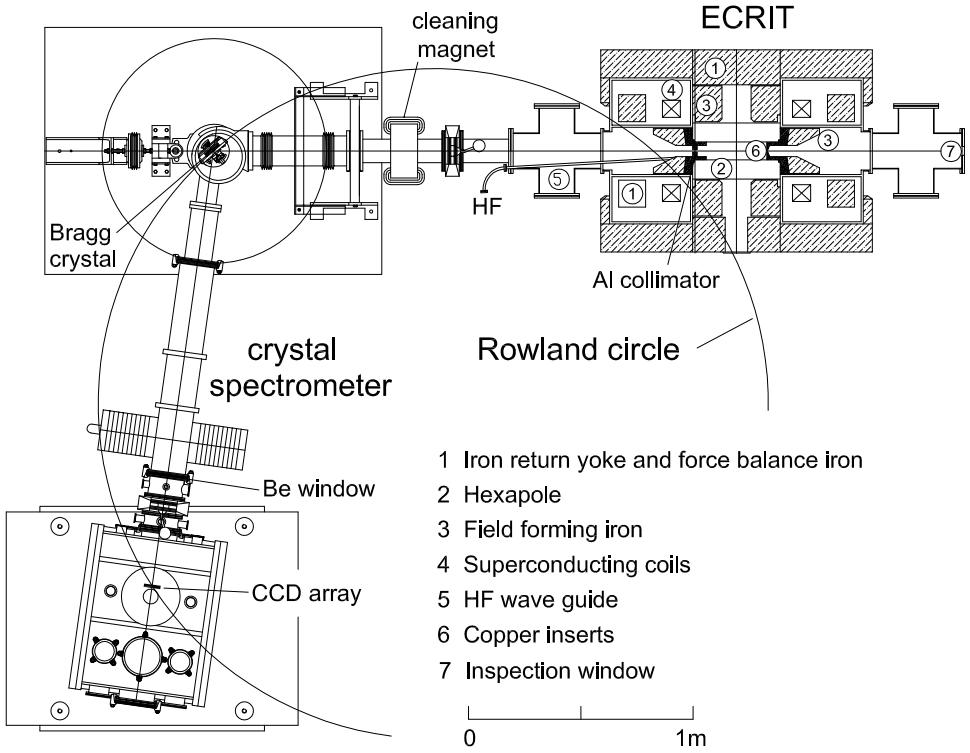

FIGURE 6. Setup of the PSI ECRIT and the Bragg crystal spectrometer (from [77]).

A permanent hexapole magnet was inserted in between the coils of the cyclotron trap to set up an electron–cyclotron resonance ion trap (ECRIT) [75]. Atoms of a dilute gas were heated and ionised by means a 6.4 GHz HF emitter coupled to the inner chamber of the ECRIT. In such a device, usually operated as a source for highly charged atoms, the ions are rather slow as measured by optical methods and, hence, no noticable Doppler broadening occurs [76]. For the large crystal bending radii used in this experiment, it turned out, that quartz and silicon behave as expected like ideal crystals and, altogether, a realistic picture is obtained from diffraction theory and ray tracing. A small additional contribution of 10–20%, described by a Gaussian, takes into account the deviation from the ideal resolution.

For the pionic–hydrogen experiment, the long–living M1 transitions in helium–like sulphur, chlorine, and argon atoms were measured (Fig. 7), the energies of which coincide almost with the energies of the πH$(2p-1s)$, πH$(3p-1s)$, and πH$(4p-1s)$ lines. With the ECRIT, an M1 intensity of up to 30000 counts per hour was achieved allowing systematic studies of focal conditions and apertures for our complete set of Bragg crystals. Energy resolutions of 400–500 meV (FWHM) were measured [77].

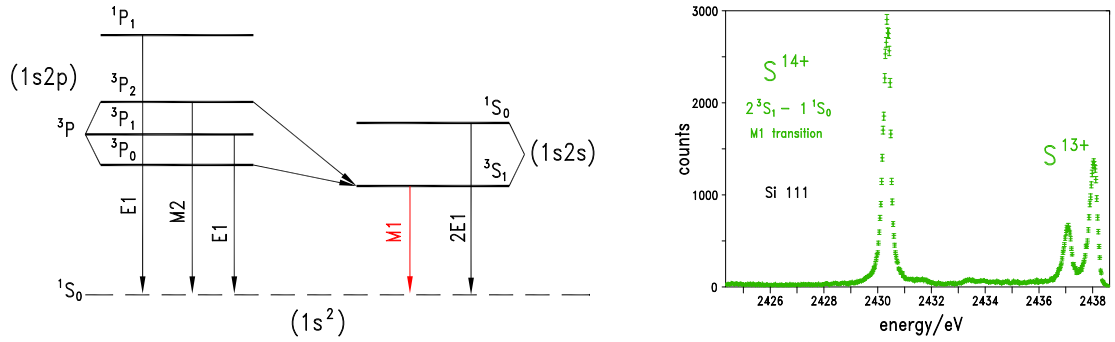

FIGURE 7. Left: level scheme of helium–like medium Z ions. Right: X–ray spectrum around the narrow M1 transition in sulphur used to calibrate the response function of the crystal spectrometer for the πH$(2p-1s)$ transition.

RESULTS

Muonic hydrogen

The line shape of the μH$(3p-1s)$ reveals directly the influence of Coulomb de–excitation by a significant broadening when compared to the response extracted from the ECRIT measurement (Fig. 8–left). In a numerical analysis three different contributions are identified: a high and medium energy component from the $(4-3)$ and $(5-4)$ Coulomb transitions and a strong low–energy part representing kinetic energies below 2 eV. The low–energy part originates from the moderation of fast μH atoms by elastic and inelastic collisions. For the μH$(3p-1s)$ transition it amounts to about 60% [79].

ESCM calculations are not able to reproduce such a high fraction of slow μH atoms, which suggests that processes during the upper part of the cascade are missing or not treated correctly. A further complication is that calculations hardly take into account the molecular structure in the μH+H_2 collisions. Therefore, present cascade calculations are not able to constrain the relative strength of the Coulomb de–excitation steps for fitting

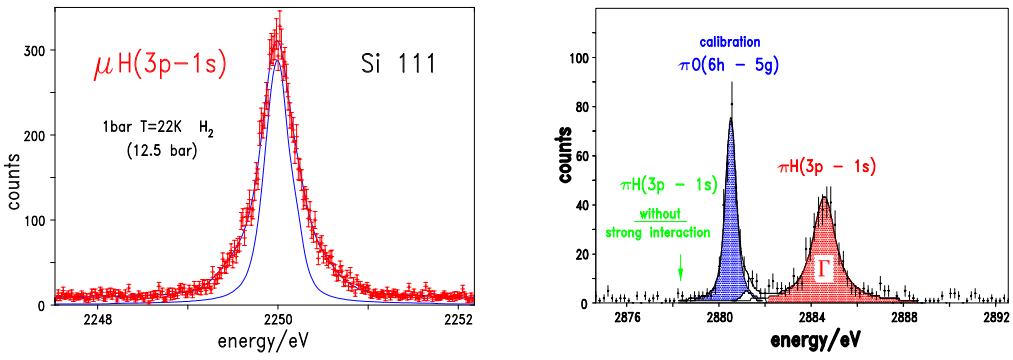

FIGURE 8. Left: muonic hydrogen – the narrow solid line corresponds to the line shape as derived from the resolution function obtained from the ECRIT measurements (from [38]). Right: pionic hydrogen – the pionic oxygen line is used for the energy calibration.

the πH X–ray line shapes. It is planned to extend the calculations to molecules and to increase the initial level to start the cascade modeling [80].

Molecular–formation calculations on the radiative de–excitation of molecular levels suggest, that satellites may appear several eV apart at the low–energy side of μH X–ray transitions, which stem from Auger stabilised molecular complexes [64]. However, no satellites are identified at the few per cent level at the low–energy side of the $\mu\mathrm{H}(3p-1s)$ transition. This is in line with the non observation of such satellites in πH.

Another result is that the μH 1s hyperfine states $^3S_1$ and $^1S_0$ are statistically populated ($\mathrm{P}(^3S_1):\mathrm{P}(^1S_0)=3{:}1$). Fitting a doublet to the line shape and fixing the hyperfine splitting to the calculated value of 183 meV [81] yields a ratio of 2.9 ± 0.3. The result confirms for the first time experimentally the assumption used in muon–capture experiments [33].

Density dependence of the transition energy

The $\pi\mathrm{H}(3p-1s)$ transition energy was measured in the a density range corresponding to hydrogen pressures from 3.5 bar to liquid (being equivalent to 700 bar). The energy was always deduced from the angular difference to the nearby $\pi^{16}\mathrm{O}(6h-5g)$ line (Fig. 8–right). No density dependence was found within the experimental accuracy. It is concluded that no radiative de–excitation occurs from molecular states. The strong–interaction shift is calculated as the weigthed average of the results for all densities [78] to be

$$\varepsilon_{1s}^{\pi H} = 7120 \pm 8\,(stat.) \pm 6\,(sys.)\ \mathrm{meV} \quad (preliminary). \tag{9}$$

The systematic uncertaintainty is dominated by the the line shape model used to fit the $\pi^{16}\mathrm{O}(6h-5g)$ line and the parallel transitions $\pi^{16}\mathrm{O}(6g-5f)$ and $\pi^{16}\mathrm{O}(6g-5d)$. Only a contribution as small as 1 meV arises from the calculation of the electromagnetic transition energy [68].

Line shape and hadronic width

With decreasing main quantum number of the X–ray transition's initial state an increasing line width is expected because additional Coulomb de–excitation steps with increasing energy gain can contribute. This picture is confirmed by the total line width increasing from the $\pi\mathrm{H}(4p-1s)$ over the $\pi\mathrm{H}(3p-1s)$ to the $\pi\mathrm{H}(2p-1s)$ transition (after subtraction of the experimental contribution). The total width of the $\pi\mathrm{H}(4p-1s)$ line constitutes already an upper limit for the hadronic broadening of $\Gamma < 850$ meV [78].

Based on the experience from the analysis of the $\mu\mathrm{H}(3p-1s)$ line shape, the Lorentzian contribution to the three πH lines measured is extracted by fitting the relative strengths of the Doppler contributions contained in these transitions. A preliminary analysis yields as weighted average (statistical error only)

$$\Gamma_{1s}^{\pi H} = 823 \pm 19\,\mathrm{meV}. \tag{10}$$

Noteworthy, that a systematic analysis of the numerical procedures revealed a strong correlation of background level and Lorentzian width leading to a systematic discrepancy. Detailed Monte–Carlo studies were performed to quantify the correction for the determination of the hadronic width. A first result is available for the πH$(4p-1s)$ line yielding $\Gamma_{1s} = 765 \pm 56$ meV, which includes a correction due to the correlation of -5% [82]. A similar analysis for the πH$(3p-1s)$ and πH$(2p-1s)$ transitions is in progress.

Pionic deuterium

In the last data taking period, the pionic deuterium $(3p-1s)$ transition was measured. Again, the pressure dependence was studied, because molecular formation calculations predict an enhanced radiative de–excitation compared to hydrogen [64]. Data were taken for 3, 10, and 30 bar equivalent density, but also in this case no energy dependence of the line energy nor satellite structures could be found. The accumulated statistics will allow to improve the accuracy for the hadronic shift and broadening from 2% to about 0.5% and from 12% to about 4%, respectively [83].

For the πD$(3p-1s)$ transition, no suitable calibration line is available from a hydrogen–like pionic atom like the combination πH/πO. Therefore, the Ga Kα_2 fluorescence line was used, which is reflected in 3^{rd} order under the same Bragg angle as the πD$(3p-1s)$ line in 1^{st} order (Fig. 9). Important was to confirm, that the tabulated value for the Ga fluorescence X–ray energy [84] was obtained with the same gallium compound (GaAs) as used in this experiment in order to avoid a possible difference of the chemical shift.

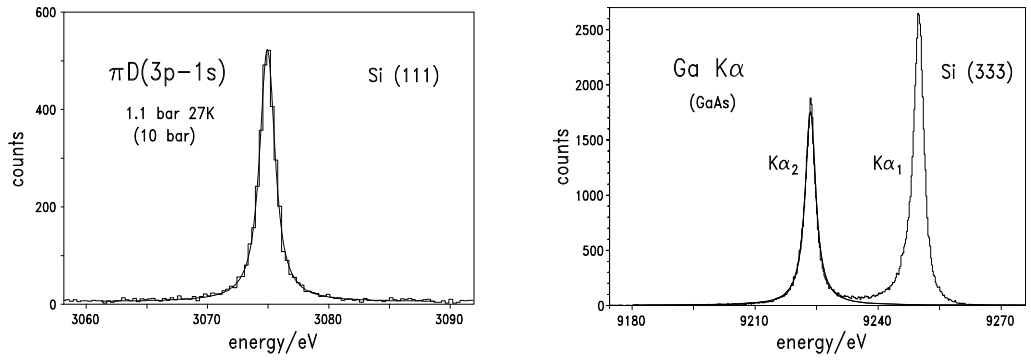

FIGURE 9. Pionic deuterium and Ga Kα_2 calibration line.

SUMMARY

A variety of techniques has been developed in the course of approaching an accurate determination of the strong–interaction effects in pionic hydrogen and deuterium. For pion beams, the cyclotron trap is essential to achieve stop densities to form a suffi-

ciently bright X–ray source suitable for ultimate–resolution spectroscopy. By using X–rays from highly charged ions, produced in a dedicated electron–cyclotron resonance source, the complex imaging properties of a Johann–type crystal spectrometer were systematically studied.

Various cascade effects have been identified and quantified in order to extract reliably hadronic shift and broadening. Coulomb explosion of molecules and Coulomb de–excitation in hydrogen have been directly observed revealing among others a still incomplete modeling of the atomic cascade.

Regarding antiprotonic atoms, the newly developed techniques will allow to achieve accuracies for strong–interaction effects comparable to the ones in pionic atoms. Cascade studies using high–resolution devices were not performed during the LEAR era. E. g., processes like Coulomb explosion are expected to be directly observable in antiprotonic atoms, in particular because Auger emission is even more efficient [85, 86]. A summary and perspectives for such kind of measurements may be found elsewhere [55, 87, 88].

In particular, the forthcoming FLAIR facility [89] is designed for antiproton fluxes comparable to the ones at LEAR being essential to resume crystal spectrometer experiments hardly possible at the AD [90], which is the only presently operating low–energy antiproton facility. In the case that ultra–low energy beam lines will be realised at FLAIR, bright X–ray sources may be achieved without using a cyclotron trap by direct injection of about 100 keV beams into a gas cell or by atomic beams crossing antiprotons stored in a trap.

ACKNOWLEDGMENTS

It is a pleasure to thank the organizers for hospitality and support during a pleasant stay (D. G.).

REFERENCES

1. S. Weinberg, Physica A **96**, 327 (1979).
2. M. Gell-Mann, R. Oakes, and B. Renner, Phys. Rev. **122**, 2195 (1968).
3. J. Gasser and H. Leutwyler, Ann. Phys. **158**, 142 (1984).
4. J. Gasser and H. Leutwyler, Nucl. Phys. B **250**, 465 (1985).
5. V. Bernard, N. Kaiser, Ulf-G. Meissner, Int. J .Mod. Phys. E **4**, 193 (1995).
6. G. Ecker, Prog. Part. Nucl. Phys. **35**, 1 (1995).
7. S. Weinberg, Phys. Rev. Lett. **17**, 616 (1966).
8. Y. Tomozawa, Nuovo Cim. A, 707 (1966).
9. T. E. O. Ericson and W. Weise, *Pions and Nuclei* (Clarendon, Oxford 1988).
10. V. Bernard, N. Kaiser, Ulf–G. Meißner, Phys. Lett. B **309**, 421 (1993).
11. V. Bernard, N. Kaiser, Ulf–G. Meißner, Phys. Rev. C **52**, 2185 (1995).
12. V. Bernard, N. Kaiser, Ulf–G. Meißner, Nucl. Phys. A **615**, 483 (1997).
13. N. Fettes, U.–G. Meißner, S. Steininger, Nucl. Phys. A **640**, 199 (1998).
14. M. Mojžiš, Eur. Phys. J. C **2**, 181 (1998).
15. N. Fettes, U.–G. Meißner, Nucl. Phys. A **676**, 311 (2000).
16. N. Fettes, U.–G. Meißner, Nucl. Phys. A **693**, 693 (2001).
17. A. W. Thomas, W. Weise, *The Structure of the Nucleon* (WILEY–VCH, Berlin 2001).

18. S. Scherer, *Introduction to Chiral Perturbation Theory*, *Advances in Nuclear Physics* **27**, ed. by J. W. Negele, E. W. Vogt (Springer, 2003).
19. S. Deser, L. Goldberger, K. Kaufmann, and W. Thirring, Phys. Rev. **96**, 774 (1954).
20. T. L. Trueman, Nucl. Phys. **26**, 57 (1961).
21. G. Rasche and W. S. Woolcock, Nucl. Phys. A **381**, 405 (1982).
22. J. Spuller et al., Phys. Lett. B **67**, 479 (1977).
23. V. E. Lyubovitskij, A. Rusetsky, Phys. Lett. B **494**, 9 (2000).
24. V. E. Lyubovitskij, Th. Gutsche, A. Faessler, R. Vinh Mau, Phys. Lett. B **520**, 204 (2001).
25. J. Gasser *et al.*, Eur. Phys. J. C **26**, 13 (2002).
26. P. Zemp, In *Proc. of Chiral Dynamics 2003*, p. 128, Bonn, Germany, September 8–13 (2003), arXiv:hep–ph/0311212v1 and 'Pionic Hydrogen in QCD + QED: Decay Width at NNLO', thesis univ. of Bern (2004).
27. T. E. O. Ericson, B. Loiseau, A. W. Thomas, Phys. Lett. B **595**, 76 (2004).
28. M. L. Goldberger, H. Miyazawa, and R. Oehme, Phys. Rev. **99**, 986 (1955).
29. T. E. O. Ericson, B. Loiseau, A. W. Thomas, Phys. Rev. C **66**, 014005 (2002).
30. V. V. Abaev, P. Metsä, and M. E. Sainio, Eur. Phys. J. A **32**, 321 (2007).
31. V. Bernard, N. Kaiser, Ulf–G. Meißner, Phys. Rev. D **50**, 6899 (1994).
32. N. Kaiser, Phys. Rev. C **67**, 027002 (2003).
33. V. A. Andreev et al., Phys. Rev. Lett. **99**, 032002 (2007).
34. V. Bernard, N. Kaiser, Ulf–G. Meißner, Phys. Lett. B **383**, 116 (1996).
35. J. Gasser, H. Leutwyler, M. P. Locher, M. E. Sainio, Phys. Lett. B **213**, 85 (1988).
36. M. E. Sainio, *Pion–nucleon σ-term – a review*, *Proc. of the 9^{th} Symp. on Meson–Nucleon Physics and the Structure of the Nucleon (MENU'01)*, *πN newsletter* **16**, 138 (2002), and references therein.
37. H.–Ch. Schröder et al., Eur. Phys. J. C **21**, 433 (2001).
38. D. Gotta et al., *Pionic Hydrogen*, Lect. Notes Phys. **745**, 165 (2008).
39. S. R. Beane, V. Bernard, T.–S. Lee, U.–G. Meißner, Phys. Rev. C **57**, 424 (1998).
40. A. Deloff, Phys. Rev. C **64**, 065205 (2001).
41. S. R. Beane, V. Bernard, E. Epelbaum, U.–G. Meißner, D. R. Phillips, Nucl. Phys. A **720**, 399 (2003).
42. B. Burasoy, H. W. Grießhammer, Int. J. Mod. Phys. E **12**, 65 (2002).
43. M. Döring, E. Oset, M. J. Vicente Vacas, Phys. Rev. C **70**, 045203 (2004).
44. U. G. Meißner, U. Raha, A. Rusetski, Eur. Phys. J. C **41**, 213 (2005).
45. U.–G. Meißner, U. Raha, A. Rusetsky, Phys. Lett. B **639**, 478 (2006).
46. U.–G. Meißner, S. Steininger, Phys. Lett. B **419**, 403 (1998).
47. V. Lensky et al., Eur. Phys. J. A **27**, 37 (2006).
48. D. Chatellard et al., Nucl. Phys. A **625**, 855 (1997).
49. P. Hauser et al., Phys. Rev. C **58**, R1869 (1998).
50. PSI experiment R-98.01, `http://www.fz-juelich.de/ikp/exotic-atoms`.
51. PSI experiment R-06.03.
52. T. B. Day, G. A. Snow, J. Sucher, Phys. Rev. Lett. **3**, 61 (1959); Phys. Rev. **118**, 864 (1960).
53. A. J. Rusi El Hassani et al., Z. Phys. A **351**, 113 (1995).
54. *Proc. of the Fifth Course of the International School of Physics of Exotic Atoms*, ed. L. M. Simons, D. Horvâth, G. Torelli, Erice, Italy, May 14–20, 1989, (Plenum Press, New York 1990), and references therein.
55. D. Gotta, Prog. Part. Nucl. Phys. **52**, 133 (2004).
56. E. Borie and M. Leon, Phys. Rev. A **21**, 1460 (1980).
57. T. S. Jensen and V. E. Markushin, Eur. Phys. J. D **19**, 165 (2002); Eur. Phys. J. D **21**, 261 (2002); Eur. Phys. J. D **21**, 271 (2002).
58. T. S. Jensen, Eur. Phys. J. D **31**, 11 (2004).
59. J. B. Czirr, Phys. Rev. **130**, 341 (1963).
60. A. Badertscher et al., Europhys. Lett. **54**, 313 (2001).
61. D. Taqqu, *Muon Catalyzed Fusion*, AIP Conference Proceedings**181**, 217 (1989).
62. S. Jonsell, J. Wallenius, P. Froelich, Phys. Rev. A **59**, 3440 (1999).
63. E. Lindroth, J. Wallenius, S. Jonsell, Phys. Rev. A **68**, 032502 (2003).
64. S. Kilic, J.–P. Karr, L. Hilico, Phys. Rev. A **70**, 052506 (2004).
65. D. F. Anagnostopoulos, D. Gotta, P. Indelicato, L. M. Simons, Phys. Rev. Lett. **91**, 240801 (2003).
66. R. Bacher et al., Phys. Rev. Lett. **54**, 2087 (1985).

67. K. Kirch et al., Phys. Rev. A **59**, 3375 (1999).
68. P. Indelicato, priv. comm.
69. T. Siems et al., Phys. Rev. Lett. **84**, 4573 (2000).
70. D. Gotta et al., Nucl. Phys. A **660**, 283 (1999).
71. L. M. Simons, Physica Scripta **T22**, 90 (1988); Hyperfine Int. **81**, 253 (1993).
72. B. Lauss et al., Phys. Rev. Lett. **80**, 3041 (1998).
73. N. Nelms et al., Nucl. Instr. Meth. A **484**, 419 (2002).
74. M. Sanchez del Rio and F. Cerrina, Rev. Sci. Instrum. **63**, 936 (1992).
75. S. Biri, L. M. Simons, D. Hitz, Rev. Sci. Instrum. **71**, 1116 (2000).
76. C. Bernard, PhD thesis, Université Claude Bernard, Lyon, 1996.
77. D. F. Anagnostopoulos et al., Nucl. Instr. Meth. A **545**, 217 (2005).
78. M. Hennebach, *Precision Measurement of Ground State Transitions in Pionic Hydrogen*, PhD thesis, Universität zu Köln, Cologne, 2003.
79. D. S. Covita et al., in preparation.
80. T. S. Jensen, V. Popov, V. Pomerant'sev, priv. comm.
81. R. N. Faustov, A. P. Martynenko, J. Exp. Theor. Phys. **98**, 39 (2004).
82. A. Hirtl, *Determination of the Strong Interaction Ground State Width in Pionic Hydrogen*, PhD thesis, Technische Universität Wien, Vienna 2008.
83. T. Strauch et al., *Proc. of 11th Int. Conference on Meson–Nucleon Physics and the Structure of the Nucleon (MENU 2007)*, to be published.
84. R. Deslattes et al., Rev. Mod. Phys., **75**, 35 (2003).
85. R. Bacher et al., Phys. Rev. A **38**, 4395 (1988).
86. D. Gotta et al., Eur. Phys. J. D **47**, 11 (2008).
87. D. Gotta, AIP conf. proc. **793**, 169 (2005).
88. H. Gorke et al., AIP conf. proc. **793**, 341 (2005).
89. *Facility for Antiproton and Ion Research*, `http://www.oeaw.ac.at/smi/flair`.
90. *The Antiproton Decelerator (AD) at CERN*, `http://psdoc.web.cern.ch/PSdoc/acc/ad`.